Mechanics Research Communications 36 (2009) 351–363

Contents lists available at ScienceDirect

Mechanics Research Communications

journal homepage: www.elsevier.com/locate/mechrescom

Derivation of Green's function using addition theorem

J.T. Chen [a,b,*], K.H. Chou [a], S.K. Kao [a]

[a] Department of Harbor and River Engineering, National Taiwan Ocean University, Keelung 20224, Taiwan
[b] Department of Mechanical and Mechanical Engineering, National Taiwan Ocean University, P.O. Box 7-59, Keelung 20224, Taiwan

ARTICLE INFO

Article history:
Received 19 May 2008
Received in revised form 23 September 2008
Available online 17 October 2008

Keywords:
Null-field integral equation
Addition theorem
Superposition
Laplace problem
Green's function

ABSTRACT

Following the success of null-field integral equation to solve the BVP of the Laplace equation, this paper employs the addition theorem and superposition technique to revisit the Green's function of Laplace problems with circular boundaries. The Green's function is decomposed into two parts, one is the fundamental solution and the other is an infinite plane of circular boundaries subject to the specified boundary conditions derived from the addition theorem. After superimposing the two solutions, the governing equation and boundary condition are both satisfied. Some examples are demonstrated to see the validity of the present method.

1. Introduction

Mathematicians as well as engineers have studied Green's functions in many fields (Jaswon and Symm, 1977; Melnikov, 1977). Green's functions are useful building blocks for attacking more realistic problems. But only a few simple regions allow a closed-form Green's function for the Laplace equation. For example, one aperture or circular sector in the half-plane, infinite strip, semi-strip or infinite wedge are mapped by elementary analytic functions, thereby enabling closed-form expressions for their Green's functions. A closed-form Green's function for the Laplace equation can be obtained by conformal mapping in this manner only in some simple cases. Numerical computation of Green's function has received attention from BEM researchers by Telles et al. (1995); Guimaraes and Telles (2000); Ang and Telles (2004)). Melnikov (1982, 1995); Melnikov and Melnikov (2001) utilized the method of modified potentials (MMP) to solve boundary value problems from various areas of computational mechanics. Later, Melnikov and Melnikov (2006) studied computing Green's functions and matrices of Green's type for mixed boundary value problems (BVP) posed on 2-D regions of irregular configuration. For the image method, Thomson (Thomson, 1848) proposed the concept of reciprocal radii to find the image source to satisfy the homogeneous Dirichlet boundary condition. Chen and Wu (2006a,b) proposed another way to find the location of image using the degenerate kernel. Chen and Ke (2008a,b) have constructed the Green's function of multiply-connected domains by using the null-field integral equation derived from Green's third identity.

In this paper, the Green's function is decomposed into two parts, one is the fundamental solution and the other is an infinite plane of circular boundaries subject to the specified boundary conditions, derived from the addition theorem. After superimposing the two solutions, the governing equation and boundary conditions are both satisfied. The main difference between the present paper and Chen and Ke (2008a,b) is that we do not directly employ Green's third identity to derive

* Corresponding author. Tel.: +886 2 24622192x6177; fax: +886 2 24632375.
E-mail address: jtchen@mail.ntou.edu.tw (J.T. Chen).

0093-6413/$ - see front matter © 2008 Elsevier Ltd. All rights reserved.
doi:10.1016/j.mechrescom.2008.10.001

the Green's function. Following the success of null-field integral equation approach for a typical boundary value problem (BVP) with Fourier boundary densities as shown in Fig. 1, it can be easily extended to derive the Green's function by introducing the superposition technique and addition theorem in the present paper. The present approach offers a few attractive

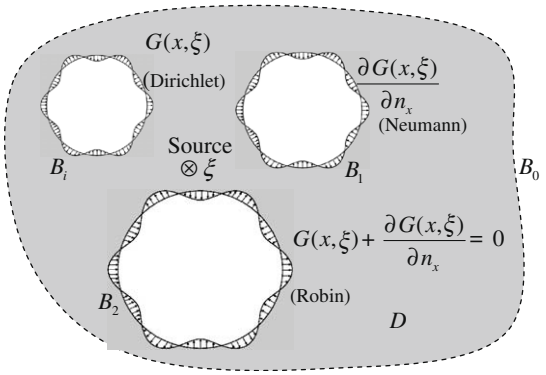

Fig. 1a. Green's function for the Laplace problem with Fourier boundary densities of the Dirichlet, Neumann and Robin types.

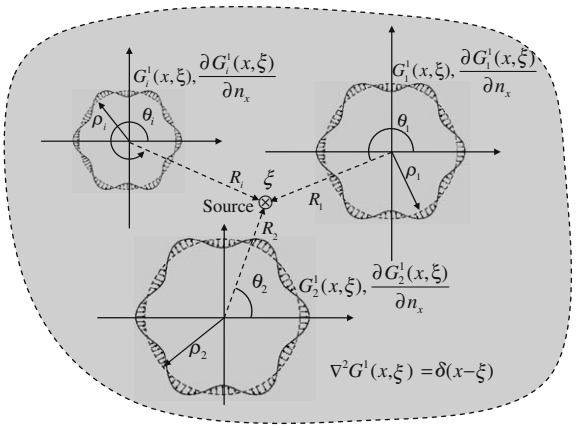

Fig. 1b. The fundamental solution for the Green's function.

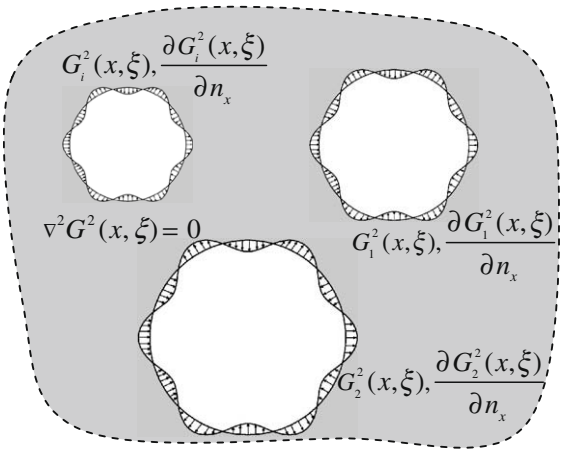

Fig. 1c. An infinite plane with circular boundary subject to the specified boundary conditions.

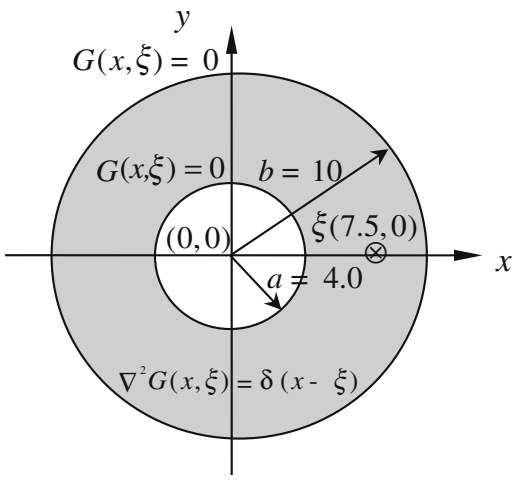

Fig. 2a. Green's function for the annular ring.

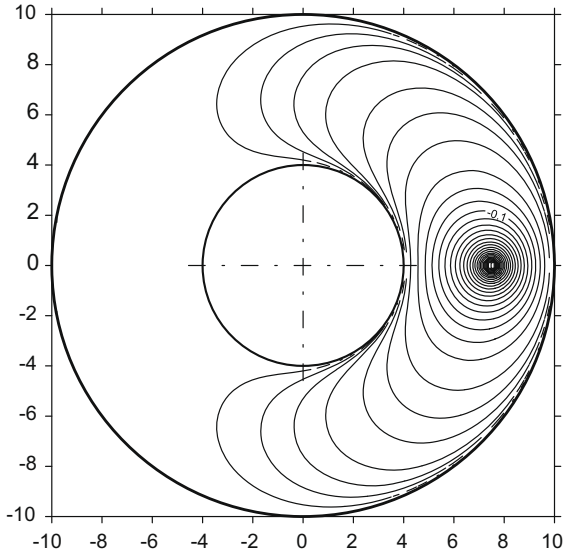

Fig. 2b. Potential contour by using the BIE approach ($M = 50$).

features. First, the integrals involved are made simple by avoiding the senses of Cauchy and Hadamard principal values. Secondly, boundary-layer effect disappears since we introduce the addition theorem for the interior and exterior regions, respectively. Finally, this method can be seen as one kind of meshless method for circular boundary since no boundary element discretization is required. Finally, some illustrative examples, annular, eccentric and half-plane cases are demonstrated to see the validity of the present method.

2. Present approach for constructing the Green's function

Considering the problem with N randomly distributed circular cavities and/or inclusions bounded in the domain D and enclosed with the boundaries, B_i ($i = 0,1,2,\ldots,N$) as shown in Fig. 1a, we define

$$B = \bigcup_{i=0}^{N} B_i \tag{1}$$

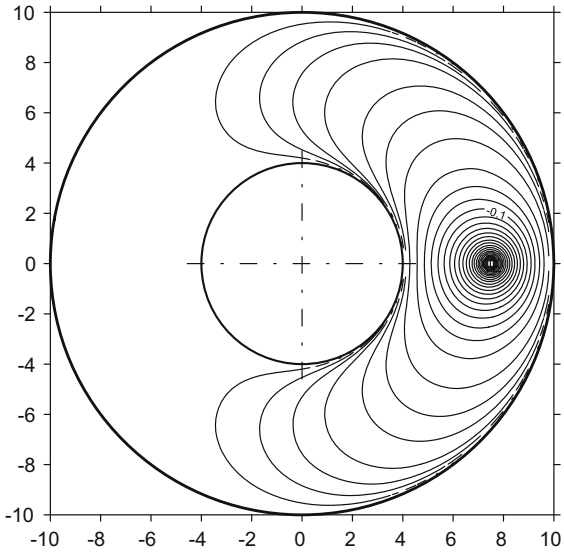

Fig. 2c. Potential contour by using the present method ($M = 50$).

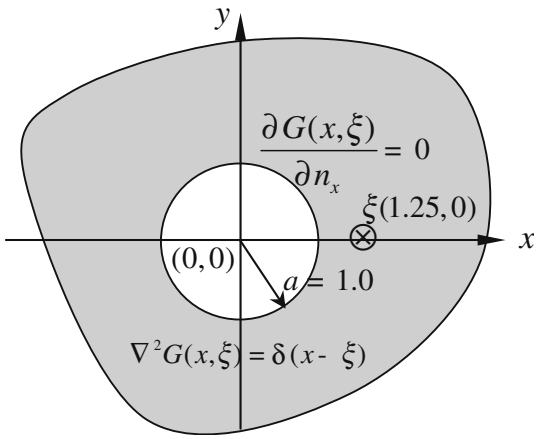

Fig. 3a. Green's function for an infinite plane with an aperture.

In mathematical physics, Green's function problems subjected to the boundary conditions and concentrated source satisfies

$$\nabla^2 G(x,\xi) = \delta(x-\xi), \quad x \in D \tag{2}$$

where $G(x,\xi)$ is the Green's function and can be seen as the potential, ∇^2 indicates the Laplacian operator. The boundary conditions of the problem are shown in Fig. 1a. Instead of using the Green's third identity in Chen and Ke (2008a,b), the problem is decomposed into two parts. One is the fundamental solution and the other is an infinite plane of circular boundaries subject to the specified boundary conditions, which are shown in Figs. 1b and 1c, respectively. For simplicity, we use the Dirichlet boundary condition ($G(\theta) = 0$) to demonstrate our formulation. The fundamental solution is governed by

$$\nabla^2 G^1(x,\xi) = \delta(x-\xi), \tag{3}$$

where $G^1(x,\xi)$ is the fundamental solution for the Laplace problem and the superscript 1 denotes the first-part solution. Based on the addition theorem, the fundamental solution can be separated into the series form in Chen and Shen (2007).

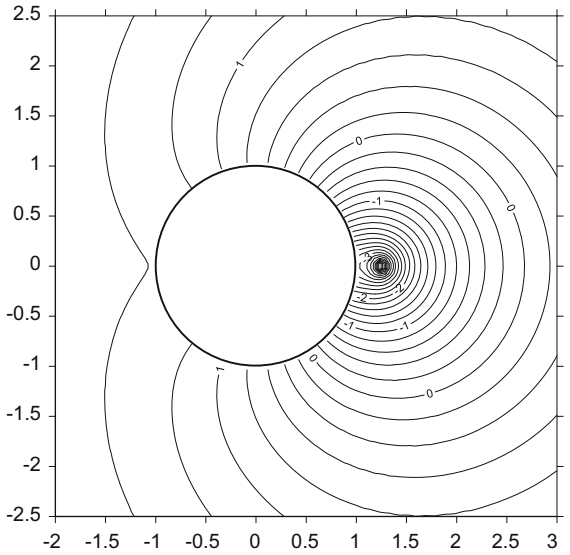

Fig. 3b. Potential contour by using the image method.

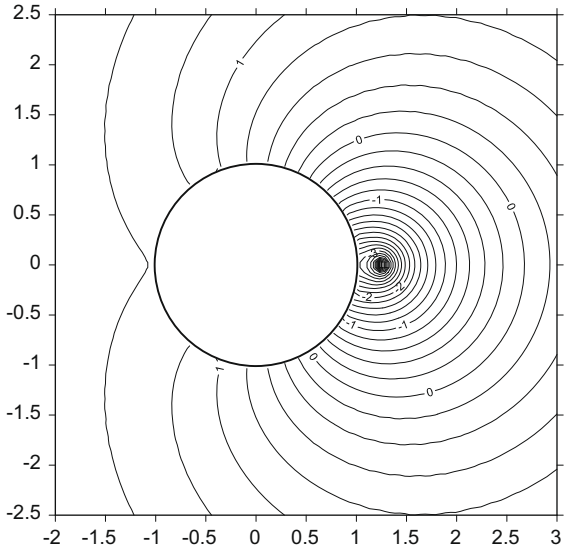

Fig. 3c. Potential contour by using the present method ($M = 50$).

To fully use the objectivity of the frame indifference, the origin of the observer system can be adaptively located on each center of the corresponding cycle.

The boundary condition along the ith circular boundary is expressed as

$$G_i^1(x,\xi) = \begin{cases} \ln R_i - \sum_{m=1}^{\infty} \frac{1}{m} \left(\frac{\rho_i}{R_i}\right)^m \cos m(\theta_i - \phi), R_i \geqslant \rho_i, \\ \ln \rho_i - \sum_{m=1}^{\infty} \frac{1}{m} \left(\frac{R_i}{\rho_i}\right)^m \cos m(\theta_i - \phi), \rho_i > R_i, \end{cases} \quad x \in B_i \tag{4}$$

where the superscript 1 of $G(x,\xi)$ denotes the first-part BC on B_i boundary due to the fundamental solution, R_i and θ_i are the distance and the polar angle between the source point and the ith center of the corresponding circle, respectively, and ρ_i is the radius of the ith cycle and B_i is the ith circular boundary. In order to satisfy the boundary condition, the second-part is a

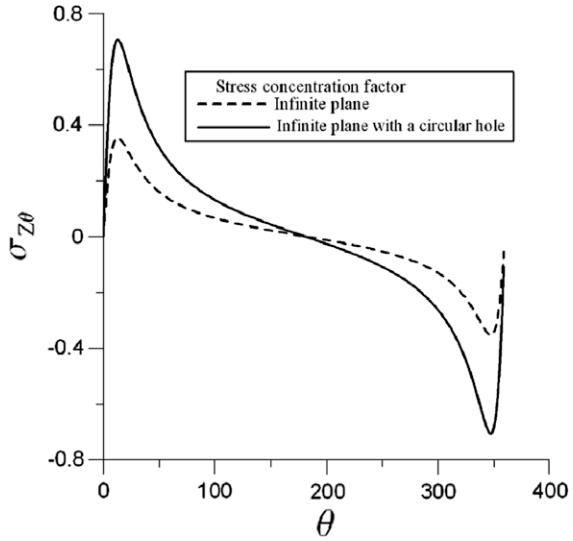

Fig. 3d. Stress distribution along the circular hole ($a = 1.0$ and $\xi = (1.25, 0)$).

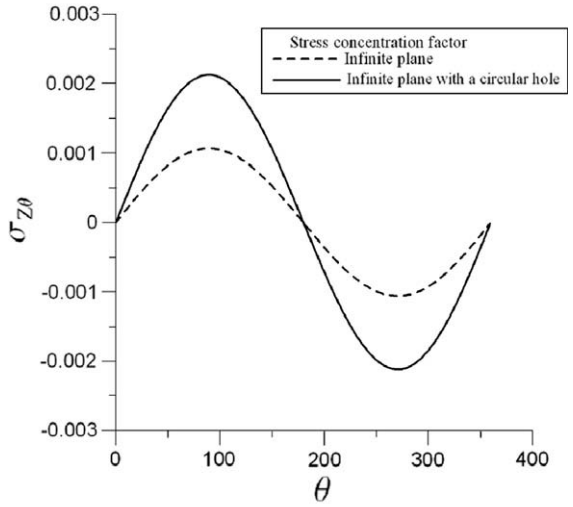

Fig. 3e. Stress distribution along the interface ($a = 1.0$ and $\xi = (150, 0)$).

typical problem subject to the specified boundary condition ($G_i^2(x,\xi) = -G_i^1(x,\xi)$) which can be expressed in terms of Fourier series after using the addition theorem.

The governing equation is shown below:

$$\nabla^2 G^2(x,\xi) = 0, \quad x \in D \tag{5}$$

where the superscript 2 denotes the second-part solution. This part can be seen as a typical BVP with circular boundaries and can be easily solved by using the null-field formulation (Chen and Shen, 2007) as shown in Fig. 1c. After superimposing the two solutions, the boundary condition automatically satisfies the Dirichlet boundary condition. Thus, the boundary condition in the second-part problem is shown below:

$$G_i^2(x,\xi) = -G_i^1(x,\xi) = \begin{cases} -\ln R_i + \sum_{m=1}^{\infty} \frac{1}{m} \left(\frac{\rho_i}{R_i}\right)^m \cos m(\theta_i - \phi), R_i \geqslant \rho_i, \\ -\ln \rho_i + \sum_{m=1}^{\infty} \frac{1}{m} \left(\frac{R_i}{\rho_i}\right)^m \cos m(\theta_i - \phi), \rho_i > R_i, \end{cases} \quad x \in B_i \tag{6}$$

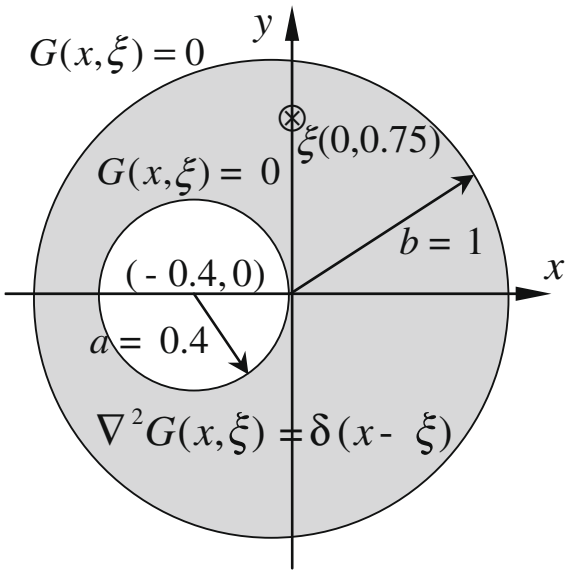

Fig. 4a. Green's function for the eccentric ring.

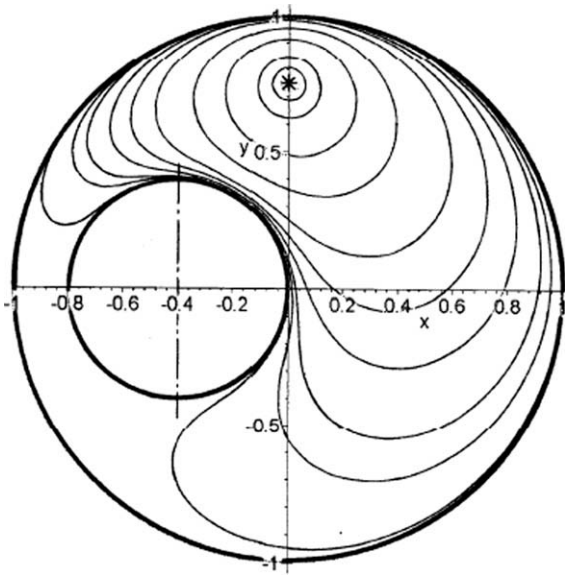

Fig. 4b. Potential contour by using the Melnikov's method (Melnikov and Melnikov, 2001).

where the superscript 2 of $G(x,\xi)$ denotes the second-part BC. By using the present approach, the problem can be solved in two stages. One is the fundamental solution (Fig. 1b) and the other is the typical BVP (Fig. 1c). After superimposing the two solutions, the Green's function can be obtained easily.

3. Numerical examples

Case1: An annular case (analytical solution)

Fig. 2a depicts the Green's function of the annular ring. The source point is located at $\xi = (7.5, 0)$. The two radii of inner and outer circles are $a = 4.0$ and $b = 10.0$. The center of the inner and outer circles is $(0, 0)$. The analytical solution is obtained as

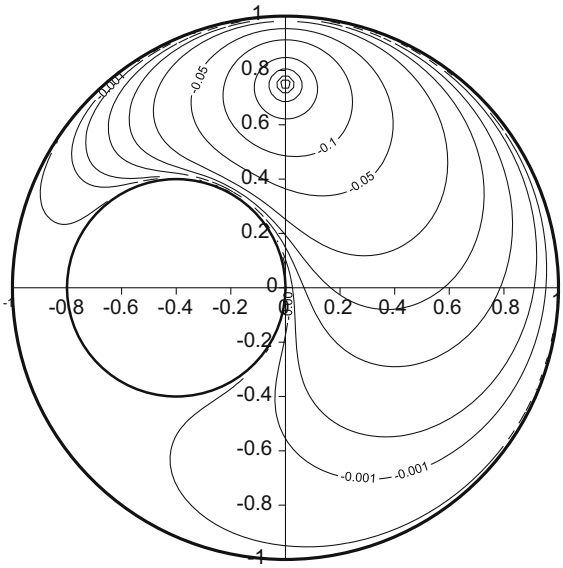

Fig. 4c. Potential contour by using the present method ($M = 50$).

$$
G(x,\xi)=\begin{cases}
G^{I}(x,\xi)=\frac{1}{2\pi}\ln R_{\xi}-\frac{1}{2\pi}\sum\limits_{m=1}^{\infty}\frac{1}{m}\left(\frac{\rho}{R_{\xi}}\right)^{m}\cos m(\theta-\phi)\\
\qquad+\frac{1}{4\pi}\sum\limits_{m=1}^{\infty}\frac{1}{m}\left(\frac{a^{2}}{\rho R_{\xi}}\right)^{m}\cos m(\theta-\phi)-a\ln\rho a_{0}\\
\qquad+\frac{1}{2}\sum\limits_{m=1}^{\infty}\frac{1}{m}\frac{a^{m+1}}{\rho^{m}}(a_{m}\cos m\phi+b_{m}\sin m\phi)-\frac{1}{2\pi}\ln b\\
\qquad+\frac{1}{4\pi}\sum\limits_{m=1}^{\infty}\frac{1}{m}\left(\frac{\rho R_{\xi}}{b^{2}}\right)^{m}\cos m(\theta-\phi)-b\ln bp_{0}\\
\qquad+\frac{1}{2}\sum\limits_{m=1}^{\infty}\frac{1}{m}\frac{\rho^{m}}{b^{m-1}}(p_{m}\cos m\theta+q_{m}\sin m\theta), \qquad R_{\xi}\geqslant\rho\geqslant a\\
G^{E}(x,\xi)=\frac{1}{2\pi}\ln\rho-\frac{1}{2\pi}\sum\limits_{m=1}^{\infty}\frac{1}{m}\left(\frac{R_{\xi}}{\rho}\right)^{m}\cos m(\theta-\phi)\\
\qquad+\frac{1}{4\pi}\sum\limits_{m=1}^{\infty}\frac{1}{m}\left(\frac{a^{2}}{\rho R}\right)^{m}\cos m(\theta-\phi)-a\ln\rho a_{0}\\
\qquad+\frac{1}{2}\sum\limits_{m=1}^{\infty}\frac{1}{m}\frac{a^{m+1}}{\rho^{m}}(a_{m}\cos m\phi+b_{m}\sin m\phi)-\frac{1}{2\pi}\ln b\\
\qquad+\frac{1}{4\pi}\sum\limits_{m=1}^{\infty}\frac{1}{m}\left(\frac{\rho R_{\xi}}{b^{2}}\right)^{m}\cos m(\theta-\phi)-b\ln bp_{0}\\
\qquad+\frac{1}{2}\sum\limits_{m=1}^{\infty}\frac{1}{m}\frac{\rho^{m}}{b^{m-1}}(p_{m}\cos m\theta+q_{m}\sin m\theta), \qquad R_{\xi}<\rho<b
\end{cases}
\tag{7}
$$

where the symbol R_{ξ} denotes the distance between the source point and the origin and the Fourier coefficients are shown below:

$$
\begin{Bmatrix}a_{0}\\a_{m}\\b_{m}\end{Bmatrix}=\begin{Bmatrix}\frac{\ln R_{\xi}-\ln b}{2\pi a(\ln a-\ln b)}\\-\frac{a^{m-1}R_{\xi}^{-m}(a^{2m}+b^{2m}-2R_{\xi}^{2m})}{2\pi(a^{2m}-b^{2m})}\cos m\theta\\-\frac{a^{m-1}R_{\xi}^{-m}(a^{2m}+b^{2m}-2R_{\xi}^{2m})}{2\pi(a^{2m}-b^{2m})}\sin m\theta\end{Bmatrix},\quad m=1,2,3,\ldots
$$

$$
\begin{Bmatrix}p_{0}\\p_{m}\\q_{m}\end{Bmatrix}=\begin{Bmatrix}\frac{\ln b-\ln R_{\xi}}{2\pi b(\ln a-\ln b)}\\\frac{b^{-m-1}R_{\xi}^{-m}(-2a^{2m}b^{2m}+(a^{2m}+b^{2m})R_{\xi}^{2m})}{2\pi(-a^{2m}+b^{2m})}\cos m\theta\\\frac{b^{-m-1}R_{\xi}^{-m}(-2a^{2m}b^{2m}+(a^{2m}+b^{2m})R_{\xi}^{2m})}{2\pi(-a^{2m}+b^{2m})}\sin m\theta\end{Bmatrix},\quad m=1,2,3,\ldots
\tag{8}
$$

Figs. 2b,2c show the potential distribution by using the BIE approach and the present method, respectively.

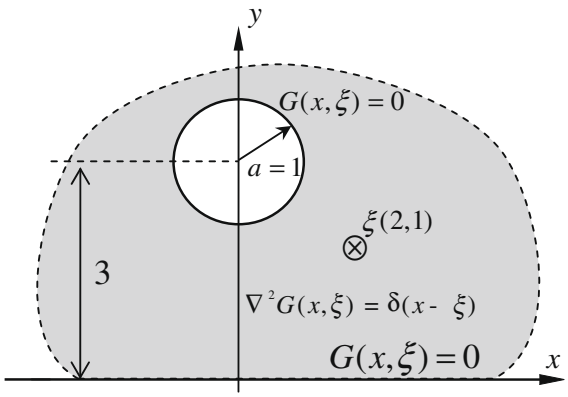

Fig. 5a. Green's function for the half-plane with the Dirichlet boundary condition.

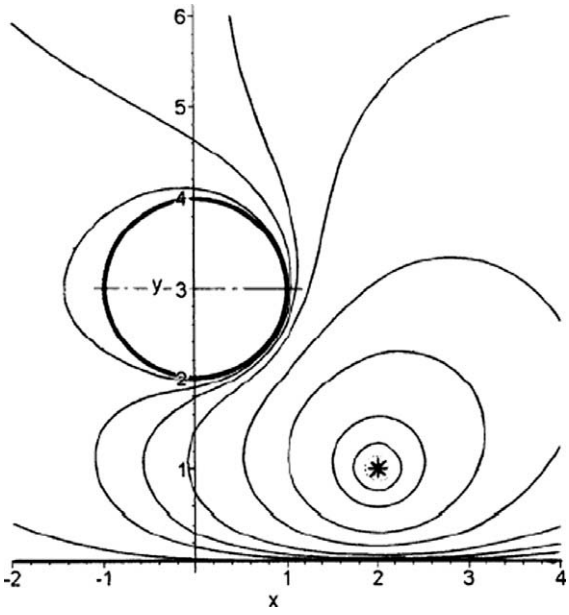

Fig. 5b. Potential contour by using the Melnikov's method (Melnikov and Melnikov, 2001).

Case 2: An infinite plane with an aperture (analytical solution)

Fig. 3a depicts the Green's function for an infinite plane with an aperture. The source point is located at $\xi = (1.25, 0)$. The center and radius of the aperture are $(0,0)$ and $a = 1.0$, respectively. By using the present formulation, the analytical solution is shown below:

$$G(x,\xi) = \begin{cases} G^I(x,\xi) = \frac{1}{2\pi}\ln R_\xi - \frac{1}{2\pi}\sum_{m=1}^{\infty}\frac{1}{m}\left(\frac{\rho}{R_\xi}\right)^m \cos m(\theta-\phi) \\ \qquad -\frac{1}{2\pi}\sum_{m=1}^{\infty}\frac{1}{m}\left(\frac{a^2}{\rho R_\xi}\right)^m \cos m(\theta-\phi), \qquad R_\xi \geqslant \rho \geqslant a \\ G^E(x,\xi) = \frac{1}{2\pi}\ln \rho - \frac{1}{2\pi}\sum_{m=1}^{\infty}\frac{1}{m}\left(\frac{R_\xi}{\rho}\right)^m \cos m(\theta-\phi) \\ \qquad -\frac{1}{2\pi}\sum_{m=1}^{\infty}\frac{1}{m}\left(\frac{a^2}{\rho R_\xi}\right)^m \cos m(\bar{\theta}-\phi), \qquad R_\xi < \rho < \infty \end{cases} \tag{9}$$

Figs. 3b and 3c show the potential distribution by using the image method and the present method, respectively. Good agreement is made. The stress distribution is shown in Figs. 3d and 3e.

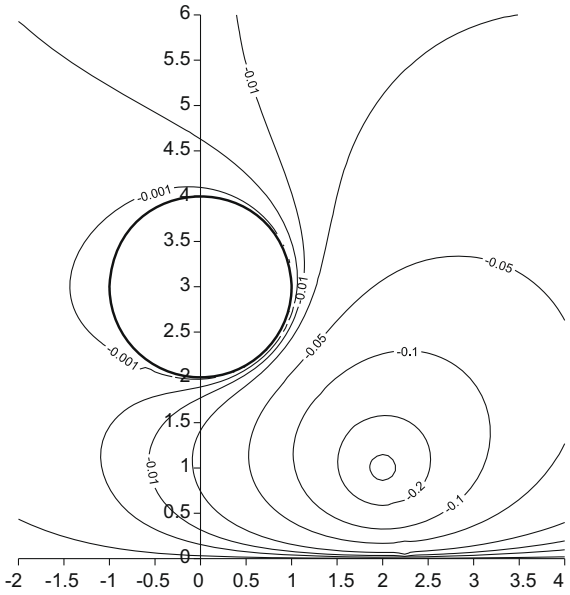

Fig. 5c. Potential contour by using the present method ($M = 50$).

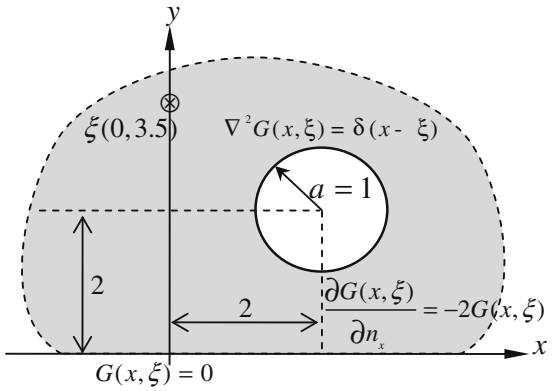

Fig. 6a. Green's function for the half-plane with the Robin boundary condition.

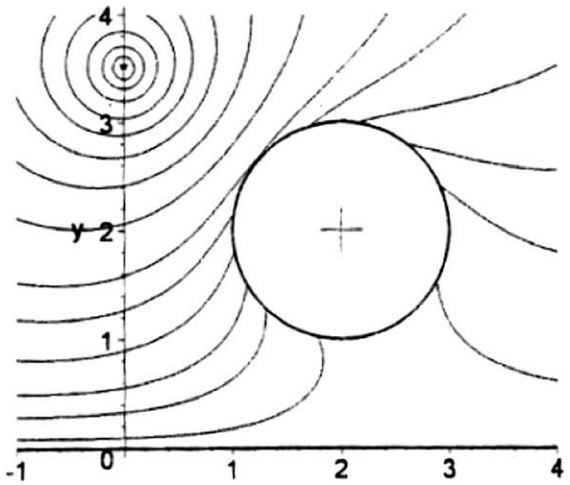

Fig. 6b. Potential contour by using the Melnikov's approach (Melnikov and Melnikov, 2006).

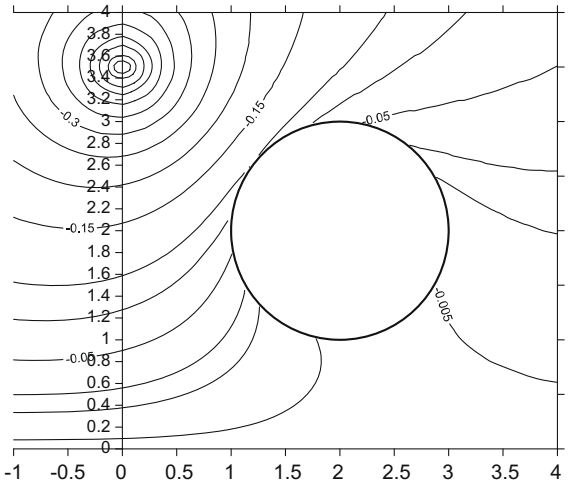

Fig. 6c. Potential contour by using the present method ($M = 50$).

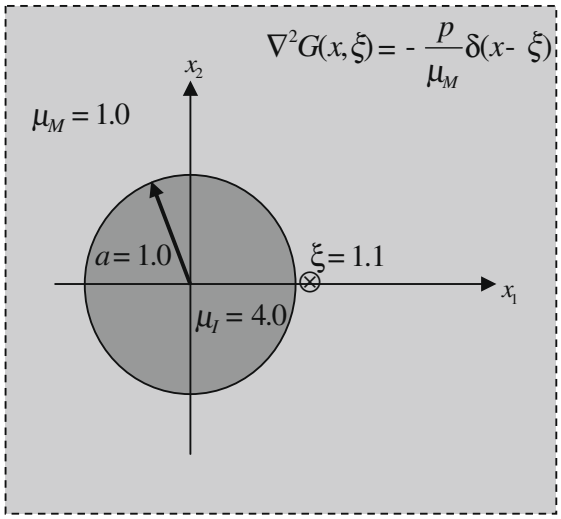

Fig. 7a. Greens function for the infinite plane with a circular inclusion.

After comparing with the two figures, we obtain the stress concentration factor of 2. When the location of the source point moving to far away, the problem can be seen as a remote shear problem with a circular hole where the concentration factor is also 2 (Chen and Wu, 2006a,b). The local maximums occur at the angles of $\frac{\pi}{2}$ and $\frac{3\pi}{2}$.

Case 3: An eccentric ring (semi-analytical solution)

Fig. 4a depicts the Green's function of the eccentric ring. The source point is located at $\xi = (0, 0.75)$. The two radii of inner and outer circles are $a = 0.4$ and $b = 1.0$. The two centers of the inner and outer circles are $(-0.4, 0)$ and $(0, 0)$, respectively. Figs. 4b and 4c show the potential distribution by using the Melnikov's approach (Melnikov and Melnikov, 2001) and the present method, respectively. We can also obtain the consistent data by using our method as well as the Green's function $G(x, \xi)$ obtained by MMP method.

Case 4: A half plane with an aperture (semi-analytical solution)

Fig. 5a depicts the Green's function for the half plane with a hole. The source point is located at $\xi = (2, 1)$. The center and radius of the aperture are $(0, 3)$ and $a = 1.0$. Figs. 5b and 5c show the potential distribution by using the Melnikov's approach and the present method, respectively. Good agreement is made.

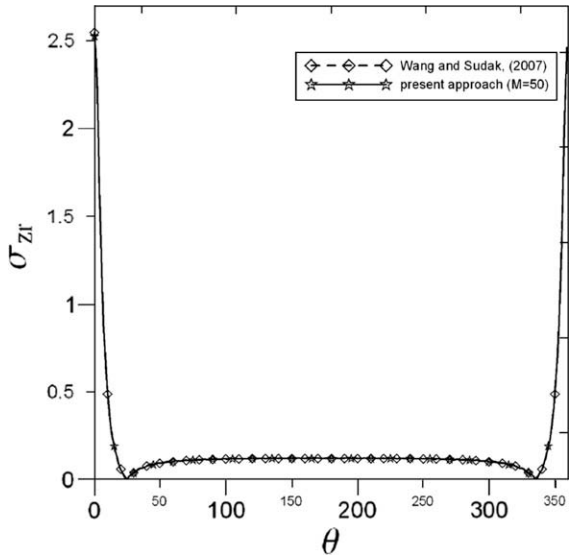

Fig. 7b. Stress distribution along the interface.

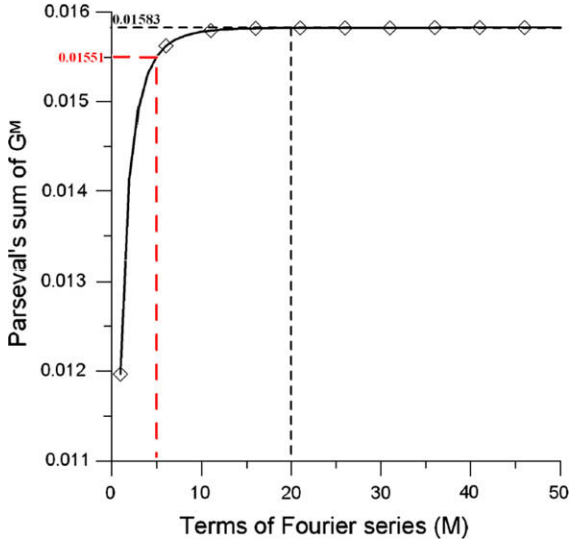

Fig. 7c. Parseval's sum for G^M with $a = 1.0$ and $\xi = (1.1, 0)$.

Case 5: A half-plane problem with a circular boundary subject to the Robin boundary condition (semi-analytical solution)

A half-plane problem with an aperture is considered. The governing equation and boundary condition are shown in Fig. 6a. The center and radius of the aperture are (2,2) and $a = 1.0$, respectively. The concentrated source is located at (0,3.5). The Robin boundary condition $\frac{\partial G(x,\xi)}{\partial n_x} = -2G(x,\xi)$ is imposed on the aperture. Fig. 6b and 6c show the potential distribution by using the Melnikov's approach and the present method, respectively. Good agreement is obtained.

Case 6: An infinite plane problem with a circular inclusion (analytical solution)

An infinite plane problem with a circular inclusion is considered. The governing equation and boundary condition are shown in Fig. 7a. The center and radius of the inclusion are (0,0) and $a = 1.0$, respectively. The concentrated source is located at (1.1,0). Fig. 7b shows the stress distribution along the interface. After comparing the result of the present approach with that of the Wang and Sudak (2007), good agreement is obtained. After using the Parseval's theorem to test the convergence rate, Figs. 7c and 7d are obtained.

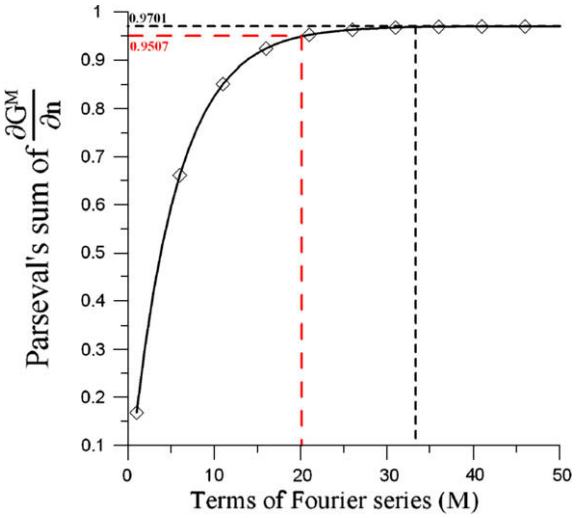

Fig. 7d. Parseval's sum for $\frac{\partial G^M}{\partial n}$ with $a = 1.0$ and $\xi = (1.1, 0)$.

4. Conclusions

For the Green's function with circular boundaries, we have proposed an indirect approach to construct the Green's function by using the addition theorem and superposition technique. Several examples, including three analytical solutions (*an annular case, an infinite plane with an aperture and an infinite plane with a circular inclusion*) and three semi-analytical solutions (*an eccentric ring, a half plane with an aperture and a half-plane problem with a circular boundary subject to the Robin boundary condition*) were demonstrated to check the validity of the present formulation. The present method has more physical sense (taking free body) to solve the Green's function for the Laplace problems with circular boundaries. Our advantages are five folds: (1) mesh-free generation (2) well-posed model (3) principal-value free (4) elimination of boundary-layer effect (5) exponential convergence.

References

Ang, W.T., Telles, J.C.F., 2004. A numerical Green's function for multiple cracks in anisotropic bodies. J. Eng. Math 49, 197–207.
Chen, J.T., Wu, C.S., 2006a. Alternative derivations for the Poisson integral formula. Int. J. Educ. Sci. Technol. 37, 165–185.
Chen, J.T., Wu, A.C., 2006b. Null-field approach for piezoelectricity problems with arbitrary circular inclusion. Eng. Anal. Bound. Elem. 30, 971–993.
Chen, J.T., Shen, W.C., 2007. Degenerate scale for multiply connected Laplace problems. Mech. Res. Commun. 34, 69–77.
Chen, J.T., Ke, J.N., 2008a. Construction of Green's function using null field integral approach for Laplace problems with circular boundaries. CMC, accepted for publication.
Chen, J.T., Ke, J.N., 2008b. Derivation of anti-plane dynamic Green's function for several circular inclusions with imperfect interfaces. CMES 29 (3), 111–135.
Guimaraes, S., Telles, J.C.F., 2000. General application of numerical Green's functions for SIF Computations with boundary elements. CMES 1 (3), 131–139.
Jaswon, M.A., Symm, G.T., 1977. Integral Equation Methods in Potential Theory and Electrostatics. Academic Press, New York.
Melnikov, Y.A., Melnikov, M.Y., 2001. Modified potential as a tool for computing Green's functions in continuum mechanics. CMES 2, 291–305.
Melnikov, Y.A., 1995. Green's Functions in Applied Mechanics. Computational Mechanics Publications, Boston, Southampton.
Melnikov, Y.A., Melnikov, M.Y., 2006. Green's functions for mixed boundary value problems in regions of irregular shape. Electron. J. Boundary Elem. 4, 82–104.
Melnikov, Y.A., 1982. A basis for computation of thermo-mechanical fields in elements of constructions of complex con figuration. Thesis Dr. Technical Sciences, Moscow Institute of Civil Engineering (in Russian).
Melnikov, Y.A., 1977. Some application of the Green's function method in mechanics. Int. J. Solids struct. 13, 1045–1058.
Telles, J.C.F., Castor, G.S., Guimaraes, S., 1995. Numerical Green's function approach for boundary elements applied to fracture mechanics. Int. J. Numer. Methods Eng. 38 (19), 3259–3274.
Thomson, W., 1848. Maxwell in his Treatise, vol. I (chapter XI, quotes a paper in the Cambridge and Dublin Math. Journ. of 1848).
Wang, X., Sudak, L.J., 2007. Antiplane time-harmonic Green's functions for a circular inhomogeneity with an imperfect interface. Mech. Res. Commun. 34, 352–358.